Mechanistic Studies Inform Design of Improved Ti(salen) Catalysts for Enantioselective [3+2] Cycloaddition

Sophia G. Robinson,[a†] Xiangyu Wu,[b†] Binyang Jiang,[b] Matthew S. Sigman,[a*] Song Lin[b*]

[a]Department of Chemistry, University of Utah, 315 South 1400 East, Salt Lake City, Utah 84112, United States

[b]Department of Chemistry and Chemical Biology, Cornell University, Ithaca, New York 14853, United States

ABSTRACT: Ti(salen) complexes catalyze the asymmetric [3+2] cycloaddition of cyclopropyl ketones with alkenes. While high enantioselectivities are achieved with electron-rich alkenes, electron-deficient alkenes are less selective. Herein, we describe mechanistic studies to understand the origins of catalyst and substrate trends in an effort to identify a more general catalyst. Density Functional Theory (DFT) calculations of the selectivity determining transition state revealed the origin of stereochemical control to be catalyst distortion, which is largely influenced by the chiral backbone and adamantyl groups on the salicylaldehyde moieties. While substitution of the adamantyl groups was detrimental to the enantioselectivity, mechanistic information guided the development of a set of eight new Ti(salen) catalysts with modified diamine backbones. These catalysts were evaluated with four electron-deficient alkenes to develop a three-parameter statistical model relating enantioselectivity to physical organic parameters. This statistical model is capable of quantitative prediction of enantioselectivity with structurally diverse alkenes. These mechanistic insights assisted the discovery of a new Ti(salen) catalyst, which substantially expanded the reaction scope and significantly improved the enantioselectivity of synthetically interesting building blocks.

INTRODUCTION

Stereoselective catalysis of radical-based organic transformations remains a challenge in modern synthetic chemistry in part due to the high reactivity and relatively limited knowledge about reaction pathways involving radical intermediates.[1] Recent advances have made possible a plethora of highly enantioselective reactions mediated by radical intermediates.[2] In contrast to the rapid developments in this area, mechanistic understanding of catalytic radical-based reactivities lags behind.[3] Better understanding will lead to rational design and optimization of next generation catalysts with broader scope and improved synthetic applications.

In this context, we have recently developed a new catalytic strategy that harnesses the single-electron redox activity of Ti complexes for the formal [3+2] cycloaddition of cyclopropyl ketones and alkenes (Figure 1).[4] Notably, the use of a chiral Ti(salen) complex ((***R,R***)-**4a**) renders this transformation diastereo- and enantioselective, producing polysubstituted cyclopentanes from alkenes and cyclopropyl ketones. This development is interesting for several reasons. Synthetically, cyclopentanes are common structures in complex bioactive compounds.[5] In particular, cyclopentylcarboxylic acids (cf. **3e** and **3f**) have been studied as structural analogs for prolines in the discovery and evaluation of peptidyl drugs.[6] On a fundamental level, enantioselective radical reactions catalyzed by Ti predominantly rely on chiral cyclopentadienyl ligands,[7] which are typically cumbersome to synthesize. The successful use of salen compounds, a class of modular chiral ligands, in enantioselective reactions will have significant implications in this burgeoning area of research.[4b]

In the initial discovery, we found that Ti catalysts such as (***R,R***)-**4a** generally promoted the reaction in excellent diastero- and enantioselectivity for styrene-type substrates with electron-rich and -neutral substituents (e.g., (***S,S***)-**3a–b**). Nonetheless, reactions with electron-deficient alkenes led to much poorer stereocontrol, and the application of lower reaction temperatures was necessary to achieve reasonable levels of enantioselectivity at the expense of longer reaction times and lower efficiency. Specifically, acrylates, methacrylates, phenyl vinyl sulfone, and vinyl pinacolboronate ester gave rise to products in high diastereoselectivity but low enantioselectivity (Figure 1, (***S,S***)-**3e–h**). Reactions using such Michael acceptors often afford more synthetically useful products. For example, acrylate-derived products (***S,S***)-**3e** and (***S,S***)-**3f** can be used as amino acid analogues in peptide synthesis,[6] while vinyl pinacolboronate ester **2h** provides product (***S,S***)-**3h** with a stereogenic C–B bond that could be further elaborated into other synthetically useful compounds.[8]

We sought to address this significant limitation of our reaction system and improve the Ti(salen) catalyst by means of probing the mechanism of stereochemical induction. Metal-salen complexes have been widely used in enantioselective catalysis in the context of small molecule[9] and polymer synthesis.[10] Empirically, several structural factors including the nature of the metal center,[11] the interplay of

steric and electronic factors garnered by the salicylaldehyde groups,[12] and the conformation of the complex[13] can profoundly influence the reaction enantioselectivity. In contrast to the extensive use of metal-salen complexes in asymmetric catalysis, mechanistic understanding of the high enantioselectivity imparted by these chiral catalysts remains largely underexplored with the exception of the extensive, elegant studies of the hydrolytic kinetic resolution of epoxides by Jacobsen.[14] Against this backdrop, we aimed to gain further insights into the mechanism of stereochemical induction in the context of the Ti-catalyzed [3+2] cycloaddition reaction with the primary goal of providing general guidelines for new catalyst design to improve currently challenging substrate classes, namely electron poor alkenes. Given the rigidity of metal salen complexes, we hope that these guidelines can be translated to other enantioselective transformations catalyzed by these privileged chiral catalysts.

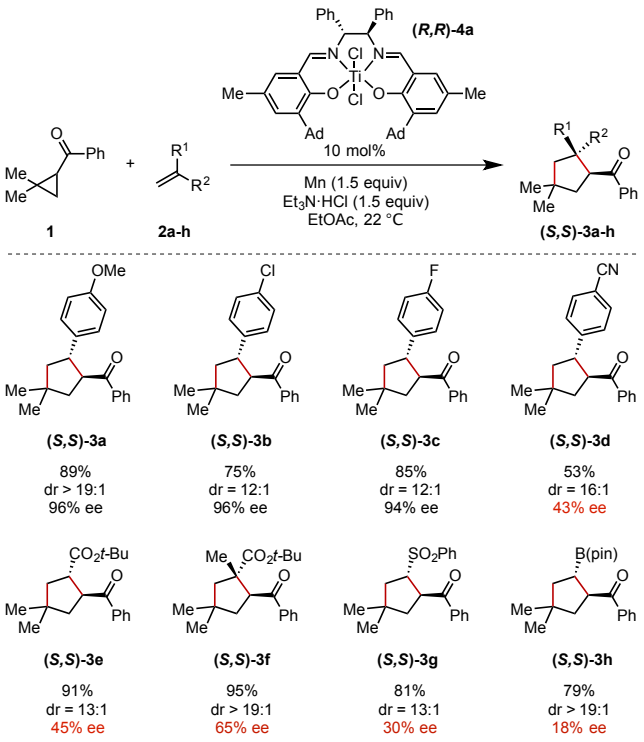

Figure 1. Reported Ti(salen) catalyzed [3+2] cycloaddition. Electron deficient alkenes yield products with lower enantioselectivies.

Thus, we report herein a combination of experimental and computational tools to interrogate the mechanism of this Ti(salen)-catalyzed [3+2] cycloaddition. Both the structural features of catalysts and substrates were systematically modified to probe structure-selectivity relationships. By combining theory and statistical mathematical modeling, a stereochemical model was developed that features the role of catalyst distortion as well as intermediate positioning provided by both the chiral diamine backbone and the *ortho*-substituents on the salicylaldehyde of the catalyst. Ultimately, this informed the design of a new catalyst, which significantly expanded and improved the scope of the reaction.

RESULTS AND DISCUSSION

A. Experimental and Computational Studies of Reaction Mechanism

The proposed mechanism for this reaction begins with the generation of an active Ti(III) catalyst via single electron reduction by Mn (Figure 2A). Subsequently, reductive ring opening of the cyclopropyl substrate occurs regioselectively under the action of the Ti(III) catalyst to yield a tertiary carbon-centered radical **I**. Addition to a radical acceptor alkene then proceeds to form intermediate **II**, which cyclizes to generate the final product. This stepwise, single-electron mechanism is supported by a spin trapping experiment (Figure 2B).[4a] Nonlinear effect and diffusion NMR experiments (see SI) were conducted to rule out cooperative reactivity between multiple catalysts, which has been reported for other metal-salen systems.[15] Diffusion NMR experiments revealed that the catalyst is monomeric in the ground state. This information, taken together with the lack of a non-linear effect of the catalytic reaction, suggests that this system operates through a monomeric catalyst. With experimental evidence to support a radical mechanism and a monomeric catalyst, computational analysis was carried out to assess the energetic feasibility of the mechanism.

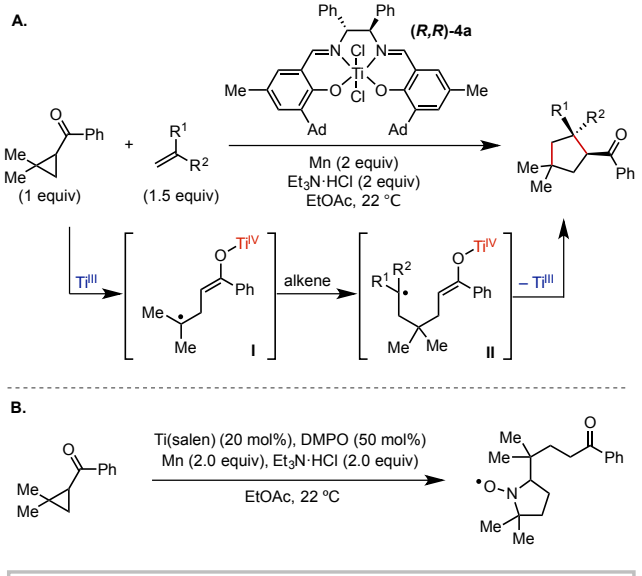

Figure 2. A. Proposed mechanism for the Ti(salen) catalyzed [3+2] cycloaddition of cyclopropylketones with alkenes, **B.** Spin trapping experiment supports a single electron mechanism.

The proposed catalytic cycle was computed using Gaussian09[16] with a model Ti catalyst with only the salen core and *p*-chlorostyrene **2b** as the substrate to reduce computational expense (Figure 3). Alternative mechanisms, such as a concerted reductive ring opening and radical addition,

were considered but such TSs were not located. As proposed, the reaction first proceeds through a TS corresponding to reductive ring opening (TS1) to yield radical intermediate **I**, which occurs with a free energy of activation of 21.0 kcal/mol relative to the catalyst-ketone complex (preTS1) and the styrene at infinite separation. The addition of this radical to the olefin (TS2) is irreversible and the rate determining step (RDS). The subsequent radical cyclization (TS3) establishes the stereogenic centers and thus is the enantio- and diastereoselectivity-determining step. With this truncated model catalyst system, the *cis* cyclization pathway is slightly lower in energy than that of the *trans*.

The achiral model catalyst allowed us to interpret the feasibility of reaction steps in the proposed mechanism, but does not explain the observed selectivities. Therefore, to interpret the origins of selectivity, computational analysis of TS3, the selectivity determining step, with the full optimal catalyst was next performed.[17]

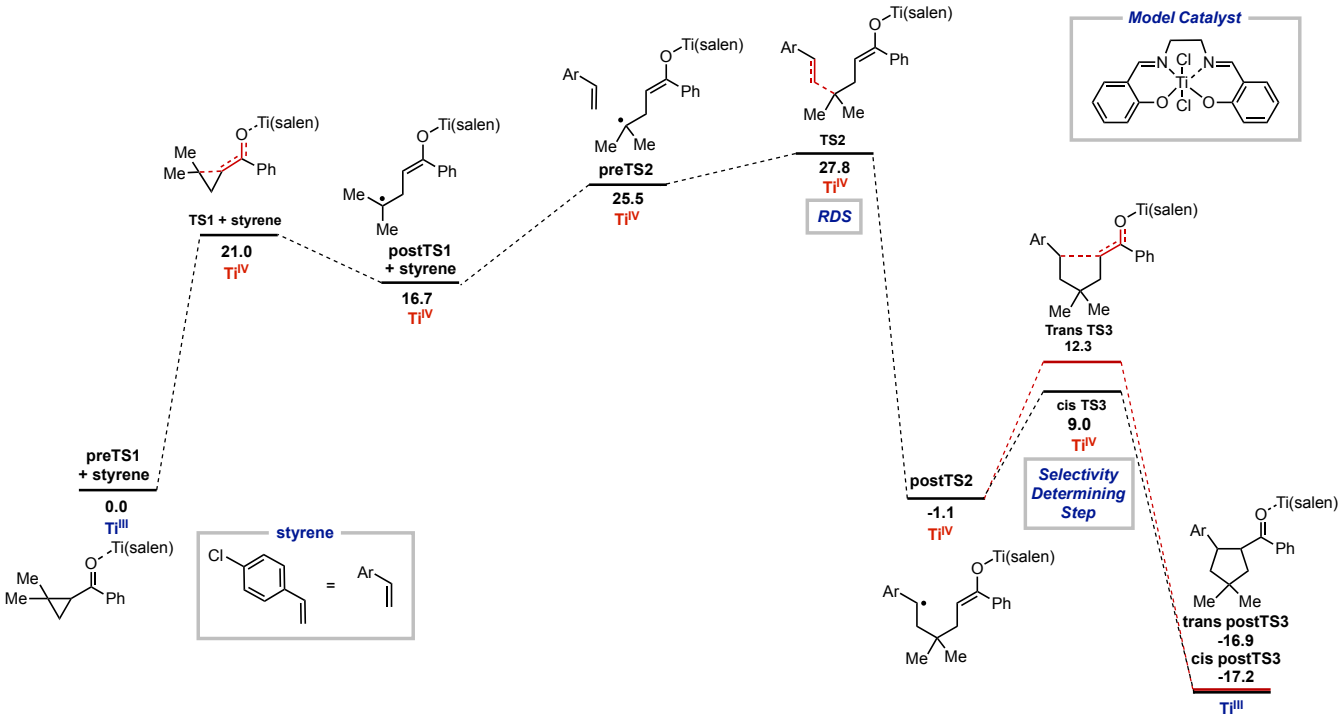

Figure 3. Catalytic cycle for the Ti(salen) catalyzed [3+2] cycloaddition calculated with a model catalyst. Energies are reported in kcal/mol. Computational method: IEFPCM(EtOAc)-M06/def2-TZVP//ωB97XD/6-31G(d)-LANL2DZ level of theory.

B. Computational Analysis of the Selectivity Determining Transition States with the Full Catalyst System

For the diastereo- and enantio-determining radical cyclization step, four possible TSs are considered: *trans*-Re, *trans*-Si, *cis*-Re, and *cis*-Si, each of which leads to a stereoisomer of the cyclopentane product. Conformers in each of these TS categories were also explored and generated by performing a conformational search (see SI for details). These conformers were then used as candidate structures for TS optimization using Gaussian09 with the IEFPCM(EtOAc)-M06/6-31+G(d,p)//M06/6-31G(d)-SDD level of theory.[16] From this process, the lowest energy structure for each of the four stereochemical pathways was interpreted further. The lowest energy pathway was calculated to be *trans*-Re TS3 (hereon referred to as major TS3), which is lower in energy by 0.8 kcal/mol relative to *cis*-Si TS3 and 1.5 kcal/mol relative to *trans*-Si TS3 (hereon referred to as minor TS3). The *cis*-Re TS3 pathway was significantly higher in energy and thus was excluded from further analysis (4.2 kcal/mol higher in energy than major TS3). These results are consistent with the experimentally observed enantio- and diastereoselectivity (Figure 4A). This method provided values in agreement with experiment for two additional styrene substrates (see SI for details), further validating the DFT method.

Visual inspection of all three TSs shows that a well-defined chiral pocket is created by the backbone and constrained by the large adamantyl groups. Conformational analysis of the catalyst core in the key TSs shows the general positions of the adamantyl groups are similar in the minor TS3 and *cis*-Si TSs, but inverted for the favored major TS3. Thus, viewing the catalyst along the C_2 axis allows for the creation of a quadrant diagram based on the general positions of the adamantyl and backbone phenyl substituents. In this diagram, two quadrants are categorized as "full" with the catalyst adamantyl and phenyl substituents positioned toward the intermediate and the other two quadrants are "empty" with the adamantyl and phenyl substituents posi-

tioned away (Figure 4B). The large steric profile of the adamantyl groups directs the intermediate to adopt a position that places aromatic substituents on the intermediate in proximity to the salen core. Therefore, the distinct catalyst conformations in each TS result in disparate contacts between catalyst and intermediate. Specifically, the qualitative model shows that the intermediate substituents are arranged in the TS that lead to competing enantiomers to occupy two full and one empty quadrants. As such, the impact of minimizing energetically repulsive contacts in one TS over another is not clear. Intriguingly, we noticed that the catalyst in the major TS3 adopts a similar planar conformation to that of the ground state of the catalyst (Figure 4C, left), whereas the catalyst is significantly distorted to a stepped conformation to form the minor or *cis*-Si TSs (Figure 4C, center and right). The differences in catalyst-intermediate arrangement and catalyst conformation prompted further assessment using distortion/interaction and noncovalent interaction (NCI) analyses to determine the stereocontrolling factors.

A distortion/interaction analysis was performed to investigate the nature and energetic cost of catalyst distortion.[18] This analysis quantifies the energy required for the catalyst and intermediate to distort into the TS conformation and the interaction energies that are established for the TS to favorably form despite the distortion. Single-point calculations in the gas-phase at the M06/6-31+G(d,p)-SDD level were employed to evaluate the relative roles of distortion and interaction on the overall energy differences for the diastereomeric TSs (see SI for computational details). Using this method, the overall energy difference for the TSs forming enantiomeric products ($\Delta\Delta E^{\ddagger}_{\text{enant.}} = \Delta E^{\ddagger}_{\text{Minor-TS3}} - \Delta E^{\ddagger}_{\text{Major-TS3}}$) and TSs forming diastereomeric products ($\Delta\Delta E^{\ddagger}_{\text{diaster.}} = \Delta E^{\ddagger}_{\textit{cis}\text{-Si-TS3}} - \Delta E^{\ddagger}_{\text{Major-TS3}}$) is 0.7 kcal/mol and 2.9 kcal/mol, respectively.[19] The calculated distortion energy differences reveal that *cis*-Re (3.1 kcal/mol) and minor (3.2 kcal/mol) TSs exhibit similar levels of distortion in reference to the major TS. Analysis of the contributions from the catalyst and intermediate fragments for each enantiomer suggests that the differences in distortion energy arise from catalyst distortion (3.09 kcal/mol)) rather than intermediate distortion (0.08 kcal/mol). Yet, the interaction energies reveal a significant difference in interaction energies for the minor TS3 relative to major TS3 (-2.5 kcal/mol), but not *cis*-Si TS3 relative to major TS3 (0.2 kcal/mol). This suggests that the interactions between catalyst and intermediate are more favorable in the minor TS3 than major TS3.

Natural energy decomposition analysis (NEDA) was performed to analyze the specific contribution of different interactions to the differences in total interaction energy for the TSs (see SI for details). While the minor TS3 has a greater level of repulsive interactions from steric crowding relative to the major TS3, minor TS3 also features more stabilizing attractive NCIs, ultimately resulting in an overall more negative total interaction energy. Furthermore, the values from this analysis imply that the *gem*-dimethyl contacts with the salen backbone in minor TS3 are more energetically costly than the interactions with the 4-chlorophenyl in major TS3. NCI plots were generated, demonstrating that a network of attractive interactions between the arenes on the intermediate and salen core occur in the TSs, further confirming our analysis (see SI).[20] Although the interaction energy for the minor TS3 is more stabilizing, the energetic penalty for distortion outweighs the stabilizing interactions. On the basis of these analyses, we propose that catalyst distortion is the major contributor to the observed stereoselectivities with the *p*-chlorostyrene substrate **2b**. The notion of a preferred conformation of a metal-salen in dictating selectivity was first invoked for rationalizing selectivity in Mn(salen)-catalyzed epoxidations, but it is plausible that catalyst distortion plays a significant role in these reactions as well.[9e, 21]

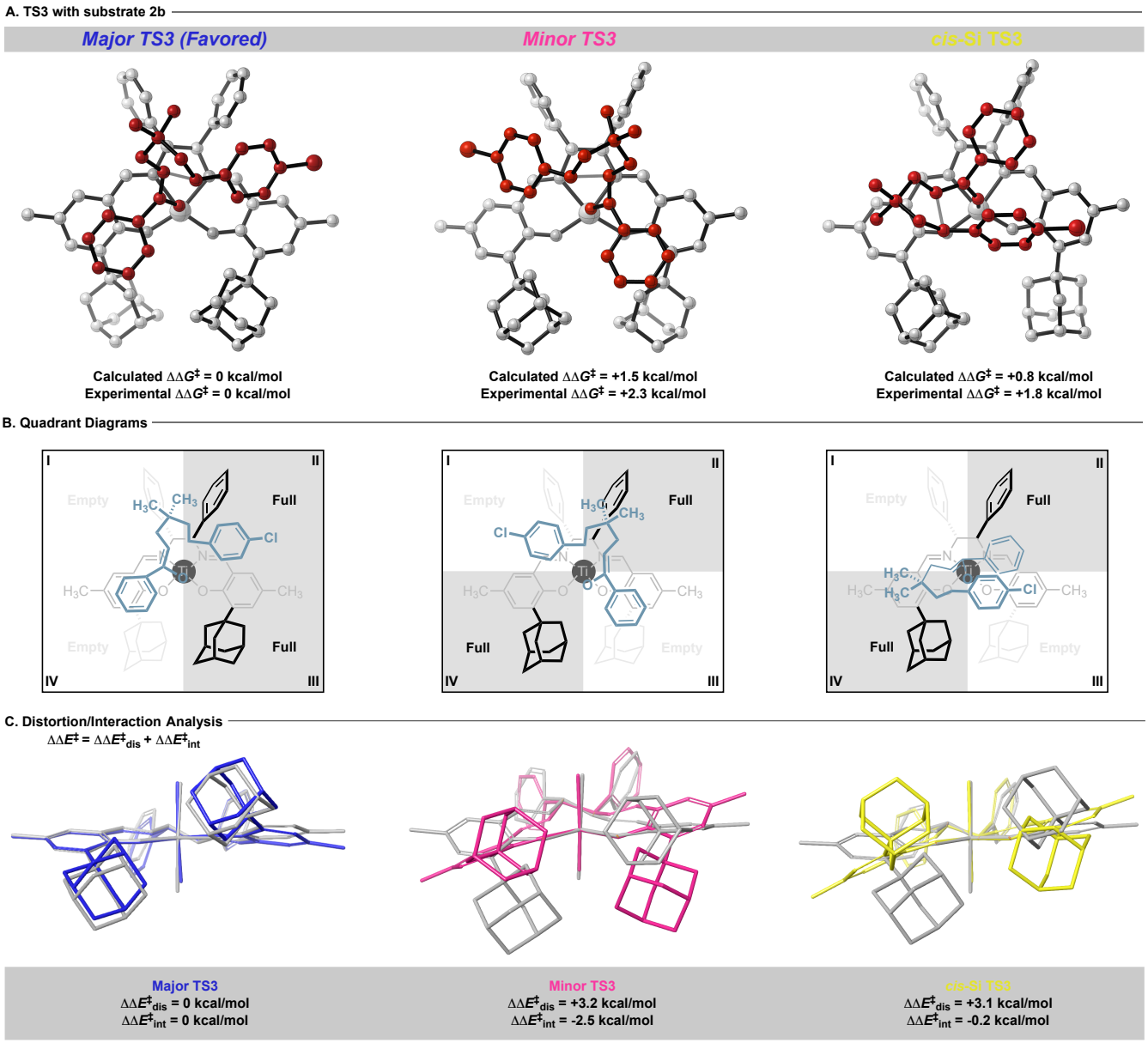

Figure 4. A. Major TS3 scenarios to consider for analysis of reaction of **2a** with (***R,R***)-**4a**, including calculated and experimental $\Delta\Delta G^{\ddagger}$ values. Computational method: IEFPCM(EtOAc)-M06/6-31+G(d,p)//M06/6-31G(d)-SDD level of theory, **B.** qualitative model developed for rationalizing selectivity outcomes based on intermediate positioning and catalyst distortion, and **C.** overlay of each catalyst TS with the lowest energy ground state catalyst (grey) to visualize catalyst distortion in each TS3. Distortion/interaction analysis was performed using single point energies calculated with M06/6-31+G(d,p)-SDD level of theory.

To determine if catalyst distortion was a stereocontrolling factor among a wider range of substrates, we next performed TS analysis with 2-vinylpyridine (**2l**). This substrate reacted to yield products in low enantioselectivity (39% ee). Since enantioselectivity, and not diastereoselecivity, was the limiting aspect of this reaction with many substrates, we focused only on TSs that form enantiomeric products. TS analysis with substrate **2l** was conducted to assess if catalyst distortion was also the primary enantiocontrolling factor with poorly performing substrates. The relevant TSs (*trans*-Re=major TS3 and *trans*-Si=minor TS3) were located using the same computational method as for the *p*-chlorostyrene TSs. The lowest energy major TS3 pathway was calculated to be 0.8 kcal/mol lower than the minor TS3 (Figure 5 top). This corresponds well with the lower levels of enantioselectivity obtained with this substrate. Distortion/interaction analysis of the TSs revealed that unlike the *p*-chlorostyrene substrate **2b**, catalyst (2.7 kcal/mol) and substrate distortion (1.0 kcal/mol) both contribute to the relative difference in distortion energy between the TSs. Since the distortion contribution (+3.7 kcal/mol) is much larger than the energy difference between the major and minor TSs, other factors must be contributing to the enantioselectivity outcome. Most notably, NEDA demonstrated that minor TS3 has a larger attractive energy term than major TS3. While these attractive inter-

actions between catalyst and intermediate lower the enantioselectivity, the overall sense of stereoinduction can be explained by catalyst distortion.

This analysis indicated that improving enantioselectivity with poorly performing substrates requires increasing catalyst distortion and/or reducing the stabilizing interactions in the minor TS3. We reasoned that modifying the catalyst structure to increase steric bulk would increase catalyst distortion.

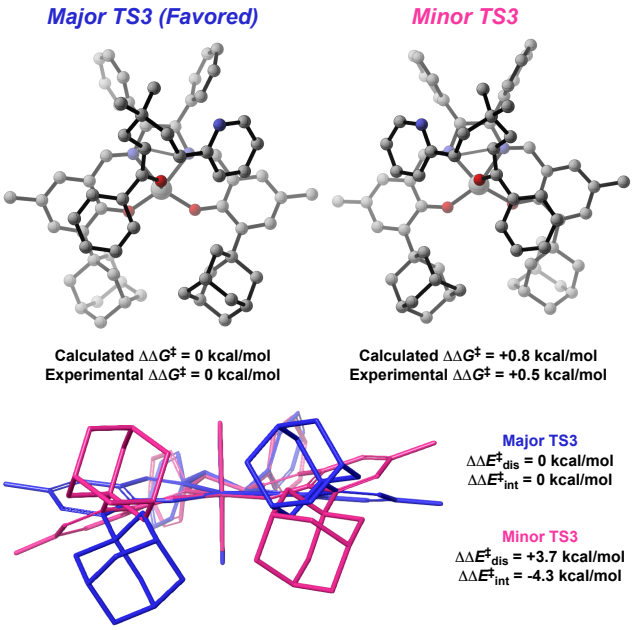

Figure 5. TS analysis for reaction of catalyst (***R,R***)-**4a** with 2-vinylpyridine **2l** as substrate (top). Distortion/interaction analysis for these TSs (bottom).

Our stereochemical models revealed that both adamantyl groups and chiral diamine backbone substituents play critical organizational roles in the selectivity-determining TS, resulting in disparate catalyst distortion. The critical role of the adamantyl groups is supported by results from a screen of a training set of Ti(salen) catalysts with variations of the salicylaldehyde portion to probe the steric influence of the *ortho* substituents and electronic tuning of the metal center by the *para* substituent. The dataset revealed large *ortho* substituents (*t*-butyl (*t*-Bu) or adamantyl (Ad)) on the catalyst are required to access enantioenriched products. Specifically, *ortho*-*t*-Bu catalysts yielded products with moderate enantioselectivities and *ortho*-Ad catalysts formed products in excellent enantio- and diastereoselectivity regardless of the *para* substituent on the catalyst (see SI for experimental details). Notably, tuning the electronics of the catalyst through the *para* substituent had a minimal effect on selectivity. Attempts to further increase the enantioselectivity by improving the size of the *ortho*-substituents beyond Ad proved unfruitful. Overall, this clearly demonstrated that varying the *ortho* and *para* substituents on the salicylaldehyde are not effective approaches for improving the catalyst, and that alternative structural modifications to the catalyst (*e.g.*, varying the diamine backbone) needed to be considered.

C. Catalyst Backbone SAR and Statistical Modeling

After our studies of structural modifications on the salicylaldehyde moiety reinforced the critical role of the adamantyl groups, we next explored introducing substituents on the diamine backbone of Ti(salen) to create a more compact stereochemical environment for the cyclization transition state to induce a higher degree of catalyst distortion in the minor TS. We note that such modifications are largely underexplored in the area of asymmetric catalysis by metal-salen complexes, despite the fact that the structure of the diamine backbone has been shown to affect enantioselectivity in certain reaction systems.[22]

As a first experimental support for the stereochemical hypothesis, we subjected a modified catalyst to the reaction in which the phenyl groups on the diamine backbone were replaced with pentafluorophenyl groups ((***S,S***)-**1aa**) (Figure 6).[23] This modification perturbs the steric and electronic environment of the active site. Indeed, the reaction with this catalyst resulted in a significant reduction of diastereo- and enantioselectivity (2:1 dr, 77% ee) relative to the parent catalyst (***S,S***)-**1aa** (14:1 dr, 90% ee; Figure 7). In the original optimization of this reaction with styrene, it was also observed that both diastereo- and enantioselectivity diminished when the phenyl diamine backbone was replaced with a cyclohexane-1,2-diamine backbone (from >19:1 to 14:1 dr, 97 to 69% ee).[4a] These results provide support that structural variation of the catalyst diamine backbone can have significant implications for stereoselectivity outcomes. Given these initial explorations did not result in a more selective catalyst, we reasoned that more subtle changes to the catalyst diamine backbone may be necessary to effectively increase catalyst distortion and reduce favorable interactions in minor TS without significantly changing the reaction pathway.

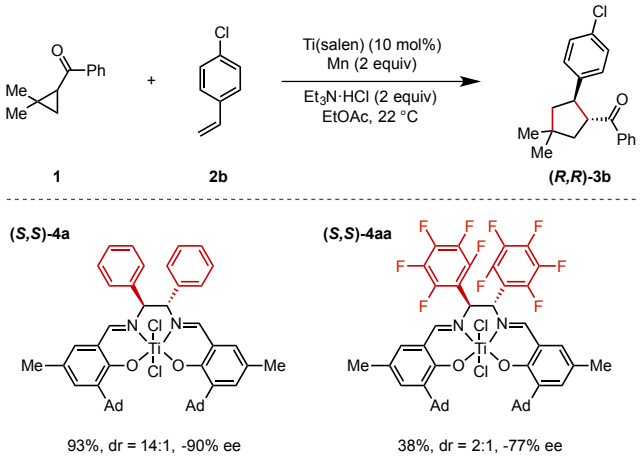

Figure 6. Modification of the chiral backbone substituents results in diminishing of stereoselectivity.[24]

Accordingly, we designed a series of eight Ti(salen) catalysts that incorporate different chiral diamine backbones ((***S,S***)-**4a**–**h**). This series of catalysts bear an *ortho* substituent on each of the aryl groups on the backbone, which

based on the computational models are perfectly positioned into the chiral pocket where the intermediate assembly is bound. Unlike (*S*,*S*)-**4aa**, these catalysts adopt a ground state conformation that is essentially identical to the parent catalyst (*S*,*S*)-**4a**. We first evaluated these catalysts in the reaction with **1** and *p*-chlorostyrene **2b**. Regardless of the backbone arene, slightly increased but comparable enantioselectivities resulted (-90 vs -93 to -96% ee; Figure 7). This result suggests that the catalyst modification did not lead to a detrimental effect on enantioinduction. We propose that the lack of sensitivity to these catalyst modifications for the styrene substrate is a consequence of similar influences on the major and minor TS3s. Essentially, comparable differences in the interplay of catalyst distortion and interaction energy result in no additional differentiation in the relative energies of these two TSs, and subsequently little influence on enantioselectivity.

In contrast, when this set of eight new Ti(salen) catalysts were explored in reactions with four electron-deficient alkene reactants, all of which performed poorly with the original optimal (***S,S***)-**4a** catalyst (Figure 7), significant enhancements were observed in enantioselectivity. Increasing the backbone steric profile results in a more confined Ti active site, thus introducing a greater degree of catalyst distortion for dictating enantioselectivity outcomes with these substrates. Initial analysis of the enantioselectivity data of the new catalyst series revealed a trend between the B5 Sterimol value of the backbone arene substituent and enantioselectivity. The size of the backbone substituent was not simply related to their efficacy, as the most selective one was neither too large nor too small. In fact, a goldilocks effect was observed in which the optimal catalyst for all four alkenes possesses the medium-sized *o*-trifluoromethylphenyl backbone substituents. Although the specific catalyst trends vary for the alkenes, catalysts with aryl backbones smaller or larger than this group yield inferior enantioselectivity outcomes (Figure 7). This suggests that smaller backbones result in inadequate levels of catalyst distortion for the minor TS3.[25] Yet, beyond a certain size the steric interactions and subsequent distortion begin to impact both the minor and major TSs, resulting in lower levels of enantioselectivity. Catalyst (***S,S***)-**4e** provides the optimal backbone to enhance catalyst distortion in the minor TS3, but not the major TS3. The results with *p*-chlorostyrene **2b** are also plotted, demonstrating the general lack of sensitivity to these structural modifications of the backbone substituent. Overall, these data provided a $\Delta\Delta G^{\ddagger}$ range of 1.5 kcal/mol, which constitutes a sufficient statistical spread to employ multivariate linear regression (MLR) statistical modeling.[26]

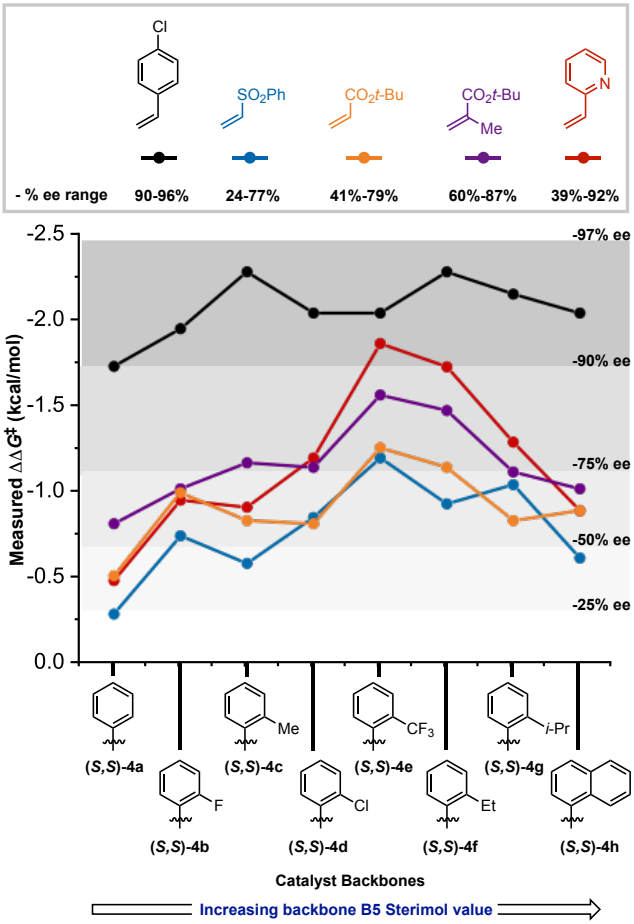

Figure 7. Graphical representation of substrate structure-selectivity trends as a function of catalyst backbone B5 Sterimol value. Each trend line represents a different olefin substrate.

MLR statistical modeling was then used to interrogate the catalyst and substrate effects specific to these alkenes. This approach relates molecular descriptor sets for the alkenes and catalysts to enantioselectivity outcomes.[26] Since the inherent enantioselectivity of the new catalysts is masked by the styrene subset in which the ee variation is small, only the substrates exhibiting variable selectivity as a function of catalyst structure were further investigated. To appropriately capture the relevant substrate features in the selectivity-determining step, parameters such as NBO charges, spin densities, and SOMO energy were acquired computationally using truncated intermediate **II** with a surrogate $TiCl_3$ in place of the full Ti(salen) catalyst. This was a simple yet crucial means of describing the molecular features most relevant to the enantio-determining step. Parameters such as Sterimol values and dihedral angles were collected from the optimized catalyst (***S,S***)-**1a–h** structures. Backbone specific parameters, such as polarizability, quadrupole moment, and molecular surface area, were obtained from the relevant arene structures and employed as additional catalyst descriptors for aiding model development. Using forward stepwise linear regression in MATLAB, a three-parameter statistical model was devel-

oped, consisting of two catalyst terms, namely polarizability and B5 Sterimol value of the arene on the diamine backbone, and one intermediate parameter, namely the NBO charge at the carbon-centered radical in intermediate **II** (Figure 8, plot I). Notably, the catalyst descriptors have larger coefficients in the model than the intermediate parameter, demonstrating the critical role of the catalyst backbone in enantioselectivity outcomes and implying significant catalyst control in this reaction. This is consistent with the proposal that catalyst distortion, as opposed to catalyst-intermediate interactions, is the primary factor in dictating enantioselectivity outcomes.

Cross-validation and external validation in which the results of all eight catalysts with a vinyl pinacolboronate ester substrate (Figure 10, **2h**) were predicted (see Figure 8 for predictions), suggest the model is robust. Furthermore, the model effectively predicted the results of three structurally diverse substrates (Figure 10, **2i**, **2j**, **2k**) with the new catalyst (***S,S***)-**4e**. The prediction for the acrylonitrile-derived product ((***R,R***)-**3i**) is less accurate, which we attribute to its substantially smaller steric profile relative to the other substrates that are more effectively modeled. All attempts at predicting results for styrene-type substrates (e.g., **2b**, **2d**, **2m**) with the model were unsuccessful and it was not possible to develop robust models when styrene substrates were included in the training set. This is consistent with the relatively flat response surface for these substrates as a function of catalyst modification and also suggests that the factors controlling enantioselectivity differ in the styrenyl substrate class.

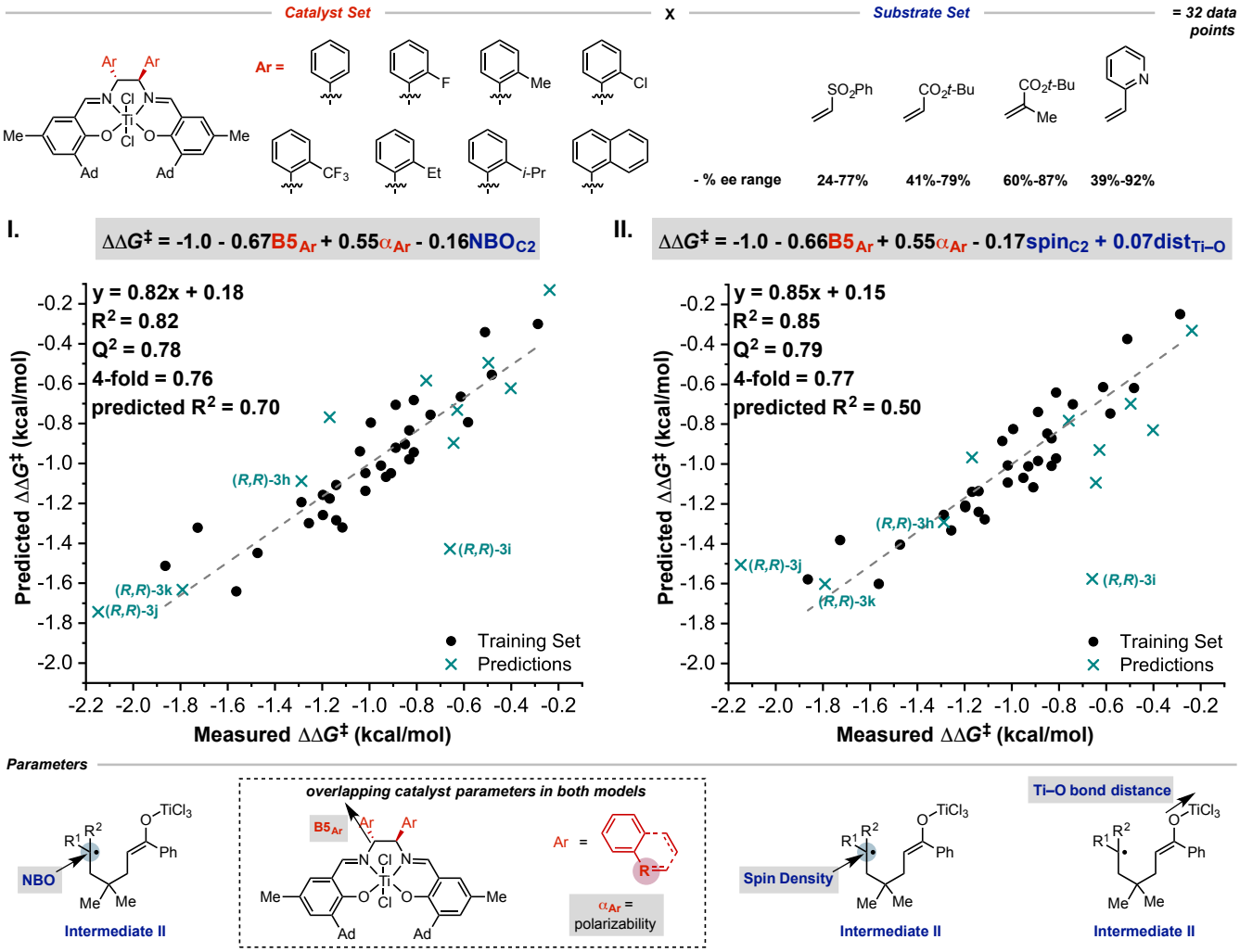

Figure 8. MLR statistical models I. and II. developed with 8 catalyst X 4 substrate matrix (32 data points for training set, top). Both models suggest there is significant catalyst control in enantioselectivity outcomes. Predictions for novel substrates with improved catalyst (***S,S***)-**1e** (Ar = *o*-CF_3Ph) are labeled. All other predictions are for product (***R,R***)-**3h** with the catalyst series.

The catalyst descriptors, polarizability and B5 Sterimol value of the aryl groups on the backbone, presumably capture the role of backbone substituents in influencing the degree of catalyst distortion (Figure 8). The two parameters are required to encapsulate the goldilocks effect of the backbone size. Intriguingly, a single parameter was sufficient at describing the diverse substrates. This is in part

due to the substantial range in these NBO charge values (-0.55 up to 0.21). Yet, interpretation of this parameter in the enantio-determining TS was unclear. Thus, our efforts focused toward developing a mechanistically interpretable model.

A correlation matrix was generated for the parameters in order to identify more digestible parameters related to the NBO_{C_2} parameter. Specifically, the spin density at the carbon centered radical ($spin_{C_2}$) and the Ti–O bond distance were determined as correlative with NBO_{C_2} of the intermediate II structures (R^2 = 0.65). Using these additional parameters, a four-parameter model was developed by manually altering the model to include these parameters in place of NBO. These two substrate parameters are interpreted as capturing the position of the TS along the reaction coordinate in the context of the Hammond postulate, in which more stabilized TSs represent more product-like TSs and result in higher levels of enantioselectivity. Although this model is more interpretable, it is less accurate in predicting out-of-sample compared to the 3-parameter model. The value of the model is the ability to quickly, computationally assess how novel substrates will perform in this reaction without requiring exhaustive TS analysis.

Yet we remained curious how the new, improved catalyst provided such marked improvements in enantioselectivity. Thus, a final set of TS analysis was performed with the 2-vinylpyridine substrate **2l** and the best catalyst ***(R,R)*-4e**. The lowest energy major TS3 pathway was calculated to be 5.0 kcal/mol lower in energy than the minor TS3 pathway (Figure 9). While the energy difference is overestimated, the reproduction of experimental enantioselectivity trends, specifically that this new catalyst **(*S,S*)-4e** should promote the reaction with 2-vinylpyriinde with higher levels of enantioselectivity than catalysts **(*S,S*)-4a**, demonstrates the strength of the computational analysis. Distortion/interaction analysis was performed with single-point energy calculations in gas phase with M06/6-31+G(d,p)-SDD level. This revealed that the distortion energy difference between the TS3s was increased (6.0 kcal/mol), while the relative interaction energy difference was reduced (-1.6 kcal/mol). This suggests that the backbone modification was an effective avenue for both increasing catalyst distortion and reducing the stabilizing interaction energy in the minor TS3.

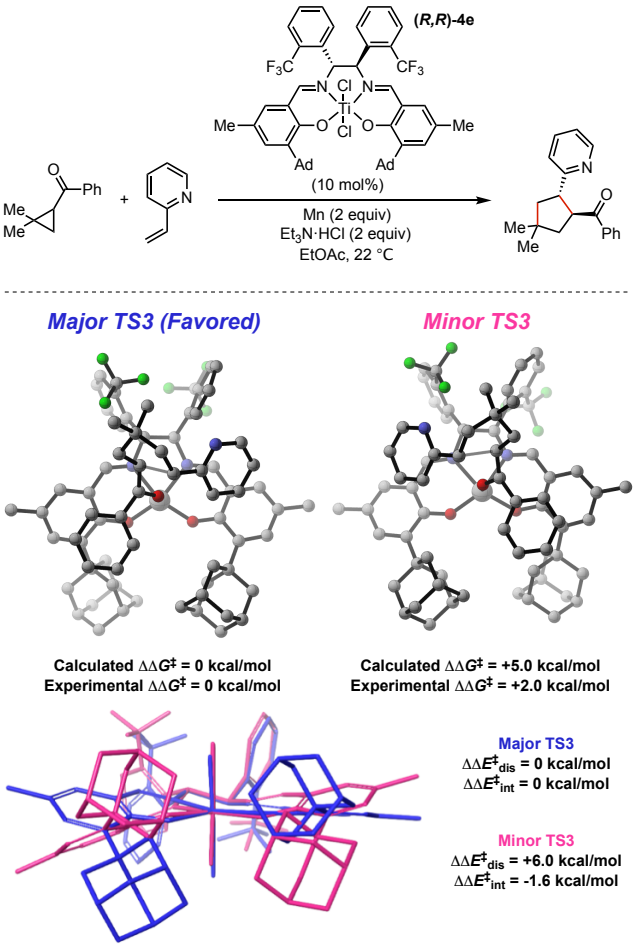

Figure 9. TS analysis for reaction of catalyst **(*R,R*)-4e** with 2-vinylpyridine **2l** as substrate (top). Distortion/interaction analysis for these TS3s (bottom).

D. Substrate Scope Expansion Using New Generation Ti(salen)

The catalyst modification informed by computational analysis led us to identify an improved Ti(salen) catalyst **(*S,S*)-4e** for the [3+2] cycloaddition reaction. Thus, the scope with the new Ti(salen) catalyst **(*S,S*)-4e** was substantially expanded to include various previously challenging, electron-deficient alkenes (Figure 10). Although the MLR statistical model and TS analysis suggests that the enantio-determining factors likely differ for styrene-type substrates from Michael acceptors, enantioselectivity was retained or improved for styrene-type substrates using the new catalyst (**(*R,R*)-3a, (*R,R*)-3b, (*R,R*)-3d** and **(*R,R*)-3m**). In other words, the new catalyst constitutes a more general catalyst for a broader range of reaction partners without compromise to the original results, a particularly challenging feat in asymmetric catalysis.

With respect to electron-deficient alkenes, the precise improvement in diastereo- and enantioselectivity varied for each substrate, with the most significant improvement being for vinyl-2-pyridine **2l**, which constituted a 1.4 kcal/mol

increase in differential free energy of activation. Notably, this improved Ti(salen) catalyst provides access to a diverse suite of synthetically useful products in high diastereo- and enantioselectivity. For example, proline analogues ((***R,R***)-**3e–f**) and a quaternary α-amino acid ((***R,R***)-**3j**) can be accessed from acrylates. Reactions with phenyl vinyl sulfone and vinyl pinacolboronate ester give rise to carbocycles with stereogenic C–S and C–B bonds (*e.g.*, (***R,R***)-**3g–h**) that can be further transformed into other useful products. Finally, several products with quaternary stereogenic centers, including a spiro-bicyclic structure ((***R,R***)-**3k**), could be readily formed from the corresponding 1,1-disubstituted alkenes with excellent stereoselectivity.

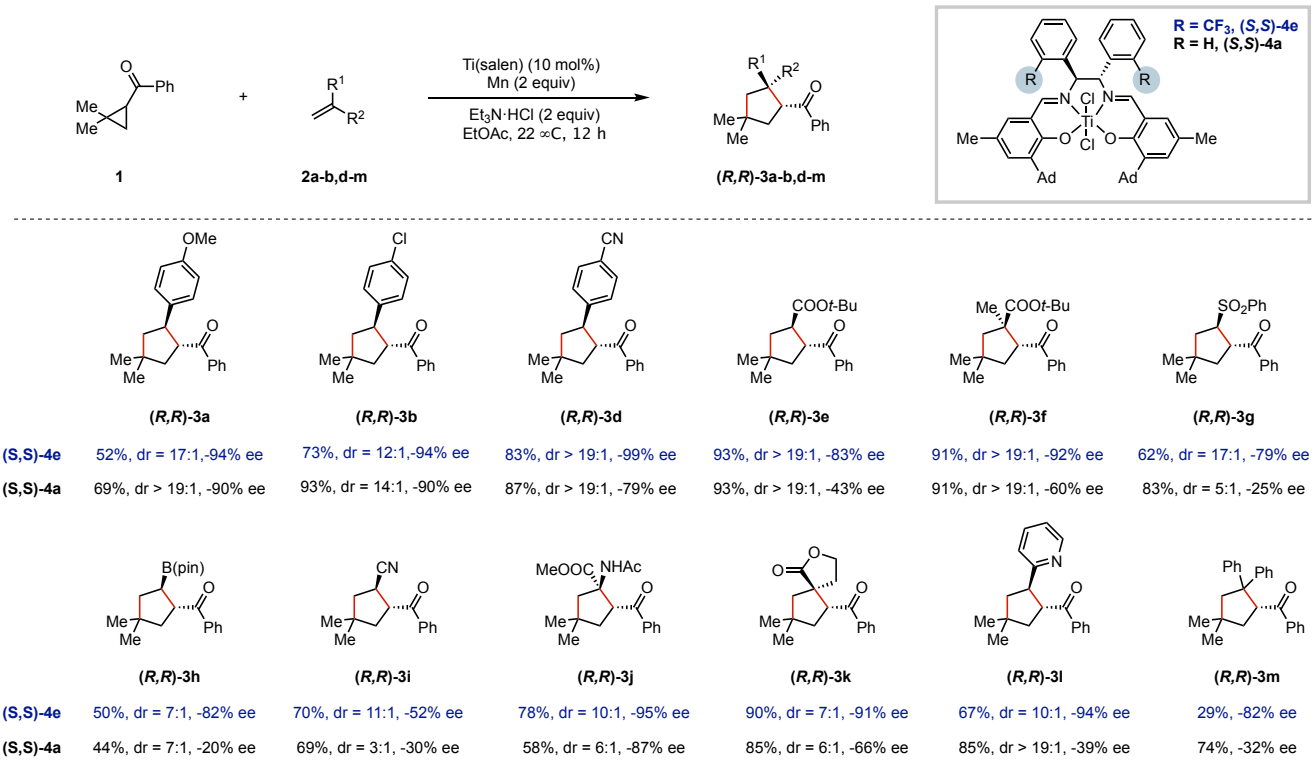

Figure 10. Improved performance of catalyst (***S,S***)-**4e** with previously challenging substrates.

CONCLUSIONS

The ability to control organic radical reactivity in a selective manner remains a synthetic challenge, but could provide access to unique useful structural scaffolds. In the Ti-catalyzed [3+2] cycloaddition reaction, through a suite of computational and experimental mechanistic studies, catalyst distortion was elucidated to dictate stereochemical outcomes. The mechanistic insights aided in our search for an improved catalyst, which substantially expanded the reaction scope and provided a collection of synthetically interesting products in high diastereo- and enantioselectivity. A catalyst-substrate matrix based on the new catalysts allowed for the development of an MLR statistical model that could predict the performance of each catalyst with a novel substrate. The predictive power of this model was demonstrated through accurate prediction of enantioselectivity outcomes for various substrates in reactions with the improved catalyst. This work demonstrates the utility of mechanistic studies in guiding catalyst optimization toward a more broadly applicable transformation. Furthermore, this development represents a rare example of metal-salen asymmetric catalysis in which the modification of the chiral diamine backbone was systematically studied to understand and improve reaction stereoselectivity. Given the broad use of metal-salen complexes in enantioselective synthesis, we anticipate that our discovery will have broader implications in transformations catalyzed by these privileged catalysts. Our future directions will focus on using the information gleaned from TS analysis to expand reactivity with different substrate classes.

ASSOCIATED CONTENT

Supporting Information

The Supporting Information is available free of charge on the ACS Publications website.

Computational details, experimental procedures, and characterization data.

AUTHOR INFORMATION

†These authors contributed equally to the work.

Corresponding Author

* songlin@cornell.edu

* sigman@chem.utah.edu

ACKNOWLEDGMENT

This work is dedicated to the occasion of Prof. Eric Jacobsen's 60th birthday and the 30th anniversary of his initial publication on Mn(salen)-catalyzed asymmetric epoxidation (commonly known as the Jacobsen epoxidation; *J. Am. Chem. Soc.* **1990**, *112*, 2801–2803). Financial support is provided by the National Science Foundation (CHE-1763436 (M.S.S)) and the National Institute of Health (GM134088 (S.L.)). Computational resources were provided from the Center for High Performance Computing (CHPC) at the University of Utah and the Extreme Science and Engineering Discovery Environment (XSEDE), which is supported by the National Science Foundation grant number ACI-1548562. SGR acknowledges the National Science Foundation for a graduate research fellowship. SGR thanks Dr. Jolene P. Reid for computational training and helpful discussions in regard to MLR modeling and TS analysis.

REFERENCES

(1) (a) Sibi, M. P.; Porter, N. A. Enantioselective Free Radical Reactions. *Acc. Chem. Res.* **1999**, *32*, 163–171. (b) Gansäuer, A.; Bluhm, H. Reagent-Controlled Transition-Metal-Catalyzed Radical Reactions. *Chem. Rev.* **2000**, *100*, 2771–2788. (c) Bar, G.; Parsons, A. F. Stereoselective Radical Reactions. *Chem. Soc. Rev.* **2003**, *32*, 251 – 263. (d) Wang, K.; Kong, W. Recent Advances in Transition Metal - Catalyzed Asymmetric Radical Reactions *Chin. J. Chem.* **2018**, *36*, 247–256. (e) Uraguchi, D.; Ohmatsu, K.; Ooi, T. Organic Molecular Catalysts in Radical Chemistry: Challenges Toward Selective Transformations. *Molecular Technology*; WileyVCH: Weinhein, 2019 Vol. 4, pp 163–197.

(2) For recent examples see: (a) Streuff, J.; Feurer, M.; Bichovski, P.; Frey, G.; Gellrich, G. Enantioselective Titanium(III) - Catalyzed Reductive Cyclization of Ketonitriles. *Angew. Chem. Int. Ed.* **2012**, *51*, 8661-8664. (b) Xu, X.; Zhu, S.; Cui, X.; Wojtas, L.; Zhang, X. P. Cobalt (II) - catalyzed asymmetric olefin cyclopropanation with α - ketodiazoacetates. *Angew. Chem. Int. Ed.* **2013**, *52*, 11857-11861. (c) Huo, H.; Shen, X.; Wang, C.; Zhang, L.; Röse, P.; Chen, L. A.; Harms, K.; Marsch, M.; Hilt, G.; Meggers, E. Asymmetric photoredox transition-metal catalysis activated by visible light. *Nature*, **2014**, *515*, 100-103. (d) Zhu, R.; Buchwald, S. L. Versatile enantioselective synthesis of functionalized lactones via copper-catalyzed radical oxyfunctionalization of alkenes. *J. Am. Chem. Soc.* **2015**, *137*, 8069-8077. (e) Zhang, W.; Wang, F.; McCann, S. D.; Wang, D.; Chen, P.; Stahl, S. S.; Liu, G. Enantioselective cyanation of benzylic C–H bonds via copper-catalyzed radical relay. *Science*, **2016**, *353*, 1014-1018. (f) Wang, Z.; Yin, H.; Fu, G. C. Catalytic enantioconvergent coupling of secondary and tertiary electrophiles with olefins. *Nature*, **2018**, *563*, 379-383. (g) Song, L.; Fu, N.; Ernst, B. G.; Lee, W. H.; Frederick, M. O.; DiStasio Jr, R. A.; Lin, S. Dual Electrocatalysis Enables Enantioselective Hydrocyanation of Conjugated Alkenes. ChemRxiv. Preprint. https://doi.org/10.26434/chemrxiv.9784625.v1 (h) Shin, N. Y.; Ryss, J. M.; Zhang, X.; Miller, S. J.; Knowles, R. R. Light-driven deracemization enabled by excited-state electron transfer. *Science*, **2019**, *366*, 364-369.

(3) For reviews on stereocontrol principles in radical reactions, see: (a) Kamigaito, M.; Satoh, K. Stereoregulation in living radical polymerization. *Macromolecules*, **2008**, *41*, 269–276. (b) Liu, L.; Ward, R. M.; Schomaker, J. M. Mechanistic Aspects and Synthetic Applications of Radical Additions to Allenes. *Chem. Rev.* **2019**, 119, 12422–12490.

(4) (a) Hao, W.; Harenberg, J. H.; Wu, X.; MacMillan, S. N.; Lin, S. Diastereo- and enantioselective formal [3+2] cycloaddition of cyclopropyl ketones and alkenes via Ti-catalyzed radical redox relay. *J. Am. Chem. Soc.* **2018**, *140*, 3514-3517. (b) McCallum, T.; Wu, X.; Lin, S. Recent Advances in Titanium Radical Redox Catalysis. *J. Org. Chem.* **2019**, *84*, 14369-14380.

(5) (a) Hudlicky, T.; Price, J. D. Anionic approaches to the construction of cyclopentanoids. *Chem. Rev.* **1989**, *89*, 1467-1486. (b) Heasley, B. Stereocontrolled preparation of fully substituted cyclopentanes: relevance to total synthesis. *Eur. J. Org. Chem.* **2009**, *2009*, 1477–1489. (c) Barrero, A. F.; Quílez, J. F.; Herrador, M. M.; Rodríguez, H.; Morales, C. P. Cyclopentane Sesquiterpenes from Fungi: Ocurrence-Bioactivity, Biosynthesis and Chemical Synthesis. *Curr. Org. Chem.* **2009**, *13*, 1164–1181.

(6) (a) Defauw, J. M.; Murphy, M. M.; Jagdmann, E., Jr.; Hu, H.; Lampe, J. W.; Hollinshead, S. P.; Mitchell, T. J.; Crane, H. M.; Heerding, J. N.; Mendoza, J. S.; Davis, J. E.; Darges, J. W.; Hubbard, F. R.; Hall, S. E. Synthesis and Protein Kinase C Inhibitory Activities of Acyclic Balanol Analogs That Are Highly Selective for Protein Kinase C over Protein Kinase A. *J. Med. Chem.* **1996**, *39*, 5215–5227. (b) Muegge, I.; Podlogar, B. L. 3D-Quantitative Structure Activity Relationships of Biphenyl Carboxylic Acid MMP-3 Inhibitors: Exploring Automated Docking as Alignment Method. *Quant. Struct. Relationships* **2001**, *20*, 215–222. (c) Stoll, V.; Stewart, K. D.; Maring, C. J.; Muchmore, S.; Giranda, V.; Gu, Y. Y.; Wang, G.; Chen, Y.; Sun, M.; Zhao, C.; et al. Influenza Neuraminidase Inhibitors: Structure-Based Design of a Novel Inhibitor Series. *Biochemistry* **2003**, *42*, 718–727. (d) Raha, K.; Merz, K. M. Large-Scale Validation of a Quantum Mechanics Based Scoring Function: Predicting the Binding Affinity and the Binding Mode of a Diverse Set of Protein-Ligand Complexes. *J. Med. Chem.* **2005**, *48*, 4558–4575. (e) Hanessian, S.; Yun, H.; Hou, Y.; Yang, G.; Bayrakdarian, M.; Therrien, E.; Moitessier, N.; Roggo, S.; Veenstra, S.; Tintelnot-Blomley, M.; et al. Structure-Based Design, Synthesis, and Memapsin 2 (BACE) Inhibitory Activity of Carbocyclic and Heterocyclic Peptidomimetics. *J. Med. Chem.* **2005**, *48*, 5175–5190.

(7) (a) Cesarotti, E.; Kagan, H. B.; Goddard, R.; Krüger, C. Synthesis of New Ligands for Transition Metal Complexes: Menthyl- and Neomenthyl-Cyclopentadienes. *J. Organomet. Chem.* **1978**, *162*, 297–309. (b) Wild, F. R. W. P.; Zsolnai, L.; Huttner, G.; Brintzinger, H. H. Ansa-Metallocene Derivatives IV. Synthesis and Molecular Structures of Chiral Ansa-Titanocene Derivatives with Bridged Tetrahydroindenyl Ligands. *J. Organomet. Chem.* **1982**, *232*, 233–247. (c) Ye, B.; Cramer, N. A Tunable Class of Chiral Cp Ligands for Enantioselective Rhodium(III)-Catalyzed C-H Allylations of Benzamides *J. Am. Chem. Soc.* **2013**, *135*, 636-639.

(8) For representative examples of stereoselective transformation of organoboron compounds: (a) Matteson, D. S.; Man, H. W.; Ho, O. C. Asymmetric Synthesis of Stegobinone via Boronic Ester Chemistry. *J. Am. Chem. Soc.* **1996**, *118*, 4560–4566. (b) Imao, D.; Glasspoole, B. W.; Laberge, V. S.; Crudden, C. M. Cross-Coupling Reactions of Chiral Secondary Organoboronic Esters with Retention of Configuration. *J. Am. Chem. Soc.* **2009**, *131*, 5024–5025. (c) Ohmura, T.; Awano, T.; Suginome, M. Stereospecific Suzuki–Miyaura Coupling of Chiral α-(Acylamino)Benzylboronic Esters with Inversion of Configuration. *J. Am. Chem. Soc.* **2010**, *132*, 13191–13193. (d) Nave, S.; Sonawane, R. P.; Elford, T. G.; Aggarwal, V. K. Protodeboronation of Tertiary Boronic Esters: Asymmetric Synthesis of Tertiary Alkyl Stereogenic Centers. *J. Am. Chem. Soc.* **2010**, *132*, 17096–17098. (e) Mlynarski, S. N.; Karns, A. S.; Morken, J. P. Direct Stereospecific Amination of Alkyl and Aryl Pinacol Boronates. *J. Am. Chem. Soc.* **2012**, *134*, 16449–16451.

(9) For reviews see following: (a) Larrow, J. F.; Jacobsen, E. N. Asymmetric Processes Catalyzed by Chiral (Salen)Metal Complexes. In *Organometallics in Process Chemistry*; Springer Berlin Heidelberg: Berlin, Heidelberg, 2004; pp 123–152. (b) Katsuki, T. Catalytic Asymmetric Oxidations Using Optically Active (Salen)Manganese(III) Complexes as Catalysts. *Coord. Chem. Rev.* **1995**, *140*, 189–214. (c) Canali, L.; Sherrington, D. C. Utilisation of

Homogeneous and Supported Chiral Metal (Salen) Complexes in Asymmetric Catalysis. *Chem. Soc. Rev.* **1999**, *28*, 85–93. (d) Jacobsen, E. N. Asymmetric Catalysis of Epoxide Ring-Opening Reactions. *Acc. Chem. Res.* **2000**, *33*, 421–431. (e) Katsuki, T. Chiral Metallosalen Complexes: Structures and Catalyst Tuning for Asymmetric Epoxidation and Cyclopropanation. *Adv. Synth. Catal.* **2002**, *344*, 131–147. (f) Bandini, M.; Cozzi, P. G.; Umani-ronchi, A. [Cr (Salen)] as a 'Bridge' between Asymmetric Catalysis, Lewis Acids and Redox Processes. *Chem. Commun.* **2002**, *9*, 919–927. (g) Katsuki, T. Some Recent Advances in Metallosalen Chemistry. *Synlett* **2003**, *3*, 281–291. (h) Cozzi, P. G. Metal – Salen Schiff Base Complexes in Catalysis: Practical Aspects. *Chem. Soc. Rev.* **2004**, *33*, 410–421. (i) McGarrigle, E. M.; Gilheany, D. G. Chromium– and Manganese–salen Promoted Epoxidation of Alkenes. *Chem. Rev.* **2005**, *105*, 1563–1602. (j) Achard, T. R. J.; Clutterbuck, L. A.; North, M. Asymmetric Catalysis of Carbon–Carbon Bond-Forming Reactions Using Metal (Salen) Complexes. *Synlett* **2005**, *12*, 1828–1847. (k) Baleiza, C.; Garcia, H. Chiral Salen Complexes: An Overview to Recoverable and Reusable Homogeneous and Heterogeneous Catalysts. *Chem. Rev.* **2006**, *106*, 3987–4043. (l) Matsumoto, K.; Saito, B.; Katsuki, T. Asymmetric Catalysis of Metal Complexes with Non-Planar ONNO Ligands: Salen, Salalen and Salan. *Chem. Commun.* **2007**, *35*, 3619–3627.

(10) For reviews see following: (a) Mackiewicz, R. M.; Phelps, A. L.; Billodeaux, D. R. Copolymerization of CO_2 and Epoxides Catalyzed by Metal Salen Complexes. *Acc. Chem. Res.* **2004**, *37*, 836–844. (b) Coates, G. W.; Moore, D. R. Discrete Metal-Based Catalysts for the Copolymerization of CO_2 and Epoxides: Discovery, Reactivity, Optimization, and Mechanism. *Angew. Chem. Int. Ed.* **2004**, *43*, 6618–6639. (c) Darensbourg, D. J. Making Plastics from Carbon Dioxide: Salen Metal Complexes as Catalysts for the Production of Polycarbonates from Epoxides and CO_2. *Chem. Rev.* **2007**, *107*, 2388–2410. (d) Osten, K. M.; Mehrkhodavandi, P. Indium Catalysts for Ring Opening Polymerization: Exploring the Importance of Catalyst Aggregation. *Acc. Chem. Res.* **2017**, *50*, 2861–2869.

(11) For representative examples see: (a) Kowalczyk, R.; Sidorowicz, Ł.; Skarżewski, J. Asymmetric Nitroaldol Reaction Catalyzed By a Chromium(III)–Salen System. *Tetrahedron: Asymmetry* **2007**, *18*, 2581–2586. (b) Sibi, M. P.; Nad, S. Enantioselective Radical Reactions: Stereoselective Aldol Synthesis from Cyclic Ketones. *Angew. Chem. Int. Ed.* **2007**, *46*, 9231–9234. (c) Mazet, C.; Jacobsen, E. N. Dinuclear {(Salen)Al} Complexes Display Expanded Scope in the Conjugate Cyanation of α, β-Unsaturated Imides. *Angew. Chem. Int. Ed.* **2008**, *47*, 1762–1765. (d) Zeng, X.; Cao, Z.; Wang, X.; Chen, L.; Zhou, F.; Zhu, F.; Wang, C.; Zhou, J. Activation of Chiral (Salen)AlCl Complex by Phosphorane for Highly Enantioselective Cyanosilylation of Ketones and Enones. *J. Am. Chem. Soc.* **2016**, *138*, 416–425.

(12) For representative examples see: (a) Palucki, M.; Finney, N. S.; Pospisil, P. J.; Güler, M. L.; Ishida, T.; Jacobsen, E. N. The Mechanistic Basis for Electronic Effects on Enantioselectivity in the (salen)Mn(III)-Catalyzed Epoxidation Reaction *J. Am. Chem. Soc.* **1998**, *120*, 948–954. (b) Bryliakov, K. P.; Talsi, E. P. Iron-Catalyzed Oxidation of Thioethers by Iodosylarenes: Stereoselectivity and Reaction Mechanism. *Chem. -Eur. J.* **2007**, *13*, 8045–8050. (c) Kull, T.; Peters, R. Contact Ion Pair Directed Lewis Acid Catalysis: Asymmetric Synthesis of *trans*-Configured β-Lactones. *Angew. Chem. Int. Ed.* **2008**, *47*, 5461–5464. (d) Park, J.; Lang, K.; Abboud, K. A.; Hong, S.; Uni, V.; Box, P. O.; Gaines, V. Self-Assembled Dinuclear Cobalt (II)-Salen Catalyst Through Hydrogen-Bonding and Its Application to Enantioselective Nitro-Aldol (Henry) Reaction. *J. Am. Chem. Soc.* **2008**, *130*, 16484–16485. (e) Kowalczyk, R.; Kwiatkowski, P.; Skarzewski, J.; Jurczak, J. Enantioselective Nitroaldol Reaction Catalyzed by Sterically Modified Salen - Chromium Complexes. *J. Org. Chem.* **2009**, *74*, 4903–4906. (f) Koya, S.; Nishioka, Y.; Mizoguchi, H.; Uchida, T.; Katsuki, T. Asymmetric Epoxidation of Conjugated Olefins with Dioxygen. *Angew. Chem. Int. Ed.* **2012**, *51*, 8243–8246. (g) Hutson, G. E.; Rawal, V. H. Salen Promoted Enantioselective Nazarov Cyclizations of Activated and Unactivated Dienones. *J. Am. Chem. Soc.* **2013**, *135*, 4988–4991.

(13) For representative examples see: (a) Belokon, Y. N.; Green, B.; Ikonnikov, N. S.; Larichev, V. S.; Lokshin, B. V; Moscalenko, M. A.; North, M.; Orizu, C.; Peregudov, A. S.; Timofeeva, G. I. Mechanistic Investigation of the Asymmetric Addition of Trimethylsilyl Cyanide to Aldehydes Catalysed by Dinuclear Chiral (Salen) Titanium Complexes. *Eur. J. Org. Chem.* **2000**, *2000*, 2655–2661. (b) Matsumoto, K.; Sawada, Y.; Saito, B.; Sakai, K.; Katsuki, T. Construction of Pseudo-Heterochiral and Homochiral Di-m-Oxotitanium (Schiff Base) Dimers and Enantioselective Epoxidation Using Aqueous Hydrogen Peroxide. *Angew. Chem. Int. Ed.* **2005**, *44*, 4935–4939. (c) Xu, Z.; Fang, R.; Zhao, C.; Huang, J.; Li, G. Cis-β-Bis (Carbonyl) Ruthenium-Salen Complexes: X-Ray Crystal Structures and Remarkable Catalytic Properties toward Asymmetric Intramolecular Alkene Cyclopropanation. *J. Am. Chem. Soc.* **2009**, *131*, 4405–4417. (d) North, M.; Watson, J. M. Asymmetric Addition of Cyanide to b -Nitroalkenes Catalysed by Chiral Salen Complexes of Titanium(IV) and Vanadium(V). *ChemCatChem* **2013**, *5*, 2405–2409.

(14) (a) Annis, D. A.; Jacobsen, E. N. Polymer-Supported Chiral Co(Salen) Complexes Mechanistic Investigations in the Hydrolytic Kinetic Resolution of Terminal Epoxides. *J. Am. Chem. Soc.* **1999**, *121*, 4147–4154. (b) Nielsen, L. P. C.; Stevenson, C. P.; Blackmond, D. G.; Jacobsen, E. N. Mechanistic Investigation Leads to a Synthetic Improvement in the Hydrolytic Kinetic Resolution of Terminal Epoxides. *J. Am. Chem. Soc.* **2004**, *126*, 1360–1362. (c) Nielsen, L. P. C.; Zuend, S. J.; Ford, D. D.; Jacobsen, E. N. Mechanistic Basis for High Reactivity of (Salen)Co-OTs in the Hydrolytic Kinetic Resolution of Terminal Epoxides. *J. Org. Chem.* **2012**, *77*, 2486–2495. (d) Ford, D. D.; Nielsen, L. P. C.; Zuend, S. J.; Musgrave, C. B.; Jacobsen, E. N. Mechanistic Basis for High Stereoselectivity and Broad Substrate Scope in the (Salen)Co(III)-Catalyzed Hydrolytic Kinetic Resolution. *J. Am. Chem. Soc.* **2013**, *135*, 15595–15608.

(15) (a) Hansen, K. B.; Leighton, J. L.; Jacobsen, E. N. On the Mechanism of Asymmetric Nucleophilic Ring-Opening of Epoxides Catalyzed by (Salen)Cr^{III} Complexes. *J. Am. Chem. Soc.* **1996**, *118*, 10924-10925. (b) Konsler, R. G.; Karl, J.; Jacobsen, E. N. Cooperative Asymmetric Catalysis with Dimeric Salen Complexes. *J. Am. Chem. Soc.* **1998**, *120*, 10780-10781.

(16) Frisch, M. J.; Trucks, G. W.; Schlegel, H. B.; Scuseria, G. E.; Robb, M. A.; Cheeseman, J. R.; Scalmani, G.; Barone, V.; Mennucci, B.; Petersson, G. A.; Nakatsuji, H.; Caricato, M.; Li, X.; Hratchian, H. P.; Izmaylov, A. F.; Bloino, J.; Zheng, G.; Sonnenberg, J. L.; Hada, M.; Ehara, M.; Toyota, K.; Fukuda, R.; Hasegawa, J.; Ishida, M.; Nakajima, T.; Honda, Y.; Kitao, O.; Nakai, H.; Vreven, T.; Montgomery Jr., J. A.; Peralta, J. E.; Ogliaro, F.; Bearpark, M.; Heyd, J. J.; Brothers, E.; Kudin, K. N.; Staroverov, V. N.; Keith, T.; Kobayashi, R.; Normand, J.; Raghavachari, K.; Rendell, A.; Burant, J. C.; Iyengar, S. S.; Tomasi, J.; Cossi, M.; Rega, N.; Millam, J. M.; Klene, M.; Knox, J. E.; Cross, J. B.; Bakken, V.; Adamo, C.; Jaramillo, J.; Gomperts, R.; Stratmann, R. E.; Yazyev, O.; Austin, A. J.; Cammi, R.; Pomelli, C.; Ochterski, J. W.; Martin, R. L.; Morokuma, K.; Zakrzewski, V. G.; Voth, G. A.; Salvador, P.; Dannenberg, J. J.; Dapprich, S.; Daniels, A. D.; Farkas, O.; Foresman, J. B.; Ortiz, J. V.; Cioslowski, J.; Fox, D. J. *Gaussian 09, Revision D.01*; Gaussian, Inc.: Wallingford, CT, **2013**.

(17) Because the selectivity-determining step occurs after the RDS, it would be difficult to experimentally study it with traditional physical organic experimental tools.

(18) (a) Champagne, P. A.; Houk, K. N. *J. Am. Chem. Soc.* **2016**, *128*, 12356-12359. (b) Bickelhaupt, F. M.; Houk, K. N. Analyzing Reaction Rates with the Distortion/Interaction-Activation Strain Model. *Angew. Chem. Int. Ed.* **2017**, *56*, 10070-10086.

(19) A variety of levels of theory were employed for identifying the optimal method for single-point energy calculations (details tabulated in SI). Electronic energies consistently underestimate the barrier for enantioselectivity and overestimate the energy barriers for diastereoselectivity regardless of the level of theory or inclusion of solvation model. Free energies for the TSs were all in reasonable agreement with experimental values, but this distortion/interaction analysis is performed using electronic energies because of the calculation of the separated distorted reactants. Thus, while the calculated dE values are not as accurate as the computed dG, the general trends for the substrate-catalyst combinations are analyzed to provide insight into this system, rather than focusing on the exact values.

(20) (a) Contreras-Garcia, J.; Johnson, E.; Keinan, S.; Chaudret, R.; Piquemal, J.-P.; Beratan, D.; Yang, W. NCIPLOT: A Program for Plotting Noncovalent Interaction Regions. *J. Chem. Theory Comput.* **2011**, *7*, 625-632. (b) Johnson, E. R.; Keinan, S.; Mori-Sanchez, P.; Contreras-Garcia, J.; Cohen, A. J.; Yang, W. Revealing Noncovlanet Interactions. *J. Am. Chem. Soc.* **2010**, *132,* 6498-6506.

(21) (a) Hashihayata, T.; Punniyamurthy, T.; Irie, R.; Katsuki, T.; Akita, M.; Moro-oka, Y. Conformational Analysis of Cationic (*R,S*)- and (*R,R*)-(Salen)manganese Complexes Possessing Axial Chirality as a Chiral Element Based on X-ray Crystallography: An Explanation of the Effect of Apical Ligand on Enantioselection by (salen)manganese Catalyst. *Tetrahedron* **1999**, *55*, 14599-14610. (b) Nishikori, H.; Ohta, C.; Oberlin, E.; Irie, R.; Katsuki, T. Mn-Salen Catalyzed Nitrene Transfer Reaction: Enantioselective Imidation of Alkyl Aryl Sulfides. *Tetrahedron* **1999**, *55,* 13937-13946.

(22) (a) Shaw, S.; White, J. D. Asymmetric Catalysis Using Chiral Salen-Metal Complexes: Recent Advances. *Chem. Rev.* **2019**, *119*, 9381-9426. (b) Discolo, C. A.; Touney, E. E.; Pronin, S. V. Catalytic Asymmetric Radical-Polar Crossover Hydroalkoxylation. *J. Am. Chem. Soc.* **2019**, *141*, 17527-17532.

(23) (a) Wheeler, S. E.; Houk, K. N. Substituent Effects in the Benzene Dimer are Due to Direct Interactions of the Substituents with the Unsubstituted Benzene. *J. Am. Chem. Soc.* **2008**, *130*, 10854-10855. (b) Cockroft, S. L.; Hunter, C. A.; Lawson, K. R.; Perkins, J.; Urch, C. J. Electrostatic Control of Aromatic Stacking Interactions. *J. Am. Chem. Soc.* **2005**, *127*, 8594-8595.

(24) Please note that the catalysts in the original method report (*J. Am. Chem. Soc.* **2018**, *140*, 3514-3517) possess (*R,R*) diamine backbones whereas catalysts with modified diamine backbones in this study were prepared with (*S,S*) diamine backbones. Thus, the (*S,S*) products formed with the (*R,R*) catalyst have positive (+) % ee, whereas performing the reaction with the (*S,S*) catalysts yields (*R,R*) products reported with negative (-) % ee values. All TS analysis was performed with (*R,R*) catalysts.

(25) Note that for the training set series the catalyst all have the (*S*,*S*) backbone whereas the original report of this method and all TS analysis employed the (*R*,*R*) backbone. Thus, for these reactions the major TS3 is *trans*-Si and the minor TS3 is *trans*-Re.

(26) For recent reviews of MLR statistical modeling see: (a) Reid, J. P.; Sigman, M. S. Comparing Quantitative Prediction Methods for the Discovery of Small-Molecule Chiral Catalysts. *Nat. Rev. Chem.* **2018**, *2*, 290-305. (b) Santiago, C. B.; Guo, J.-Y.; Sigman, M. S. Predictive and Mechanistic Multivariate Linear Regression Models for Reaction Development. *Chem. Sci.* **2018**, *9*, 2398-2412. (c) Sigman, M. S.; Harper, K. C.; Bess, E. N.; Milo, A. The Development of Multidimensional Analysis Tools for Asymmetric Catalysis and Beyond. *Acc. Chem. Res.* **2016**, *49*, 1292-1301.

Insert Table of Contents artwork here